Naval Research Laboratory

Washington, DC 20375-5000

Diffusion Fields in a Toroidal Conducting Shell of Circular Cross Section

D. DIALETIS,* L. K. LEN,[†] J. GOLDEN,[††] AND C. A. KAPETANAKOS

Beam Physics Branch
Plasma Physics Division

*Science Applications International, Inc.
1710 Goodridge Drive
P.O. Box 1303
McLean, VA 22102

[†]FM Technologies, Inc.
10529-E Braddock Road
Fairfax, VA 22032

[††]Berkeley Research Associates
P.O. Box 852
Springfield, VA 22150

October 1, 1990

REPORT DOCUMENTATION PAGE

Public reporting burden for this collection of information is estimated to average 1 hour per response, including the time for reviewing instructions, searching existing data sources, gathering and maintaining the data needed, and completing and reviewing the collection of information. Send comments regarding this burden estimate or any other aspect of this collection of information, including suggestions for reducing this burden, to Washington Headquarters Services, Directorate for Information Operations and Reports, 1215 Jefferson Davis Highway, Suite 1204, Arlington, VA 22202-4302, and to the Office of Management and Budget, Paperwork Reduction Project (0704-0188), Washington, DC 20503

1. AGENCY USE ONLY (Leave blank)	2. REPORT DATE 1990 October 1	3. REPORT TYPE AND DATES COVERED Interim

4. TITLE AND SUBTITLE

Diffusion Fields in a Toroidal Conducting Shell of Circular Cross Section

5. FUNDING NUMBERS

TA - RR011-09-41
WU - 1485
TA - XF-11133
WU - 2835

6. AUTHOR(S)

D. Dialetis,* L. K. Len,† J. Golden,†† and C. A. Kapetanakos

7. PERFORMING ORGANIZATION NAME(S) AND ADDRESS(ES)

Naval Research Laboratory
Plasma Physics Division
Code 4795
Washington, DC 20375-5000

8. PERFORMING ORGANIZATION REPORT NUMBER

NRL Memorandum Report 6719

9. SPONSORING/MONITORING AGENCY NAME(S) AND ADDRESS(ES)

Office of Naval Research
Arlington, VA 22217-5000

10. SPONSORING/MONITORING AGENCY REPORT NUMBER

11. SUPPLEMENTARY NOTES

*Science Applications International, Inc., McLean, VA 22102, †FM Technologies, Inc., Fairfax, VA 22032, ††Berkeley Research Associates, Springfield, VA 22150

12a. DISTRIBUTION/AVAILABILITY STATEMENT

Approved for public release; distribution unlimited.

12b. DISTRIBUTION CODE

13. ABSTRACT (Maximum 200 words)

The diffusion of an external magnetic field through a toroidal conducting shell is studied under the assumption of a small aspect ratio. The external magnetic field can have an arbitrary field index and magnetic flux on the minor axis of the torus. The diffused field, field index, magnetic flux and wall current are computed analytically and compared with the numerical results from the TRIDIF code. The analytical and numerical results are in good agreement. Measurements in the toroidal chamber of the NRL modified betatron gave a delay time of 34 μsec, which is less than 10% from the theoretical prediction of 37 μsec.

14. SUBJECT TERMS	15. NUMBER OF PAGES
Magnetic field diffusion, Toroidal accelerators, Modified betatron	33

16. PRICE CODE

17. SECURITY CLASSIFICATION OF REPORT	18. SECURITY CLASSIFICATION OF THIS PAGE	19. SECURITY CLASSIFICATION OF ABSTRACT	20. LIMITATION OF ABSTRACT
UNCLASSIFIED	UNCLASSIFIED	UNCLASSIFIED	UL

CONTENTS

Distribution/
Availability Codes
Avail and/or
Special

A-1

iii

DIFFUSION FIELDS IN A TOROIDAL CONDUCTING SHELL OF CIRCULAR CROSS SECTION

I. Introduction

Over the years abundant analytical work has been done on the diffusion of the magnetic field in hollow circular cylindrical conductors of infinite length[1-3], and has led to the understanding of the diffusion process in such a geometry. Much less attention has been given to the diffusion of fields in toroidal vessels. As a rule, the diffusion problem through toroidal chambers is more complex than through cylindrical conductors. The difficulty in toroidal geometry is due mainly to the application of the boundary conditions in the inner and outer surfaces of the torus. However, when the wall thickness of the torus becomes small in comparison to its minor radius, i.e., for a conducting shell, then the problem simplifies considerably. The toroidal shell approximation has been used to compute analytically the magnetic field of two toroidal segments, that carry known time independent currents. In this paper, we have extended the work of P. Rolicz et al.[4] to study the diffusion of fields through toroidal conducting shells.

The analytic results are further simplified under the additional assumption of a small aspect ratio toroidal conducting shell. To the lowest order on the aspect ratio, our work indicates that the diffusion of fields through a conducting shell of conductivity σ, major radius r_0, minor radius a and thickness d_w, depend on three characteristic times τ_0, τ_1 and τ_2, where $\tau_1 = \mu_0 \sigma a d_w / 2$ (diffusion time), $\tau_0 = 2\tau_1 [\ell n(8r_0/a) - 2]$ (L/R time), and $\tau_2 = \tau_1/2$. In contrast, the diffusion process in cylindrical shells depends on a single characteristic time (τ_1).

It is well known that there is a time lag between the magnetic field in the interior of the conducting shell and the externally applied magnetic field. This time lag can be easily measured in the laboratory and therefore is a useful physical quantity. When the transient phase of the diffusion process is over, the time lag becomes independent of time and is called the delay time τ_d. For a linearly rising applied magnetic field the delay time for a cylindrical conducting shell is equal to τ_1. On the other hand, in a toroidal conducting shell the delay time depends on both τ_0 and τ_1 and also on the flux condition, i.e., the ratio of the average field to the local field on the minor axis. Specifically $\tau_d = (\tau_0 + 3\tau_1)/2$ for the special case of a field that satisfies the betatron flux condition, i.e., when the value of the flux condition is equal to two.

In contrast to the field, the current flowing on the wall of the conducting shell depends only on τ_0. Thus, by measuring experimentally the delay time of the fields and also the rise time of the wall current, all characteristic times can be determined.

The results of the analysis have been compared with the predictions of the two-dimensional finite difference numerical code TRIDIF[5]. The agreement between theory and numerical computation is fairly good, in spite of the fact that the theory was done for a toroidal conducting shell, while in the numerical computation the torus had finite thickness. Specifically, the delay time predicted by the analysis is approximately 5% longer than the prediction of the code. Similarly, the temporal profile of the wall current from the analysis and the TRIDIF code agree to within a few percent. However, the temporal profile of the external field index and flux predicted by the theory and the code are in good agreement after a few delay times but not initially.

The delay time predicted by the theory and the code has been compared with the delay time measured in the toroidal chamber of the NRL modified betatron. For the parameters of the NRL device, the computed delay time is 37 μsec, while the measured delay time is 34 μsec. The less than 10% difference between the two delay times is probably within the uncertainty of the measurement.

In Section II, the theory is developed and a comparison is made with the numerical results obtained from the TRIDIF code. Section III contains a description of the NRL toroidal device and of the coils that generate the external magnetic field, and the measured quantities are compared with the theoretical results. Finally, in Section IV, the conclusions are presented.

II. Theory and Comparison with Numerical Results

The diffusion fields are computed near the minor axis of the circular cross section, toroidal conducting shell. As shown in Figure 1, the conductor has a major radius r_0, a minor radius a, wall thickness d_w, where $d_w << a$, and conductivity σ. In the presence of an external magnetic field which is axisymmetric and time-dependent, the diffused magnetic field inside the conductor is described by the diffusion equation

$$\vec{\nabla} \times \vec{\nabla} \times \vec{A} = -\mu_0 \sigma \frac{\partial \vec{A}}{\partial t}, \tag{1}$$

where the vector potential $\vec{A}$ has only one nonzero component A_θ that depends only on the cylindrical components (r, z) and on the time. The magnetic field components are given by

$$B_r = -\frac{\partial A_\theta}{\partial z}, \tag{2a}$$

$$B_z = \frac{1}{r} \frac{\partial r A_\theta}{\partial r}, \tag{2b}$$

2

while the electric field is equal to

$$E_\theta = -\frac{\partial A_\theta}{\partial t}.$$ (3)

Equation (1) is identical to Ampere's law combined with Ohm's law inside the conductor. In the special case, when the toroidal conductor is a shell, i.e., when $d_w << a$, this equation can be integrated and provides the first boundary condition, i.e.,

$$\vec{n} \times (\vec{B}^{out} - \vec{B}^{in}) = \mu_0 \sigma d_w \vec{E}^{in},$$ (4)

where $\vec{n}$ is the unit vector normal to the conducting wall and directed towards the region outside the conductor and μ_0 is the permeability of the vacuum. The second boundary condition is obtained from the requirement that the electric field is continuous across the boundary, i.e.,

$$\vec{E}^{in} = \vec{E}^{out}.$$ (5)

For a small aspect ratio a/r_0 vessel, it is appropriate to use toroidal coordinates. The cylindrical coordinates (r, z) are related to the toroidal coordinates (η, ξ) by:

$$r = b\frac{\sinh \eta}{\cosh \eta - \cos \xi},$$ (6a)

$$z = b\frac{\sin \xi}{\cosh \eta - \cos \xi},$$ (6b)

where b is a constant. These relations can be easily inverted, namely:

$$e^{-2\eta} = \left(\frac{r_1}{r_2}\right)^2 = \frac{(r-b)^2 + z^2}{(r+b)^2 + z^2},$$ (7a)

$$e^{-\eta} \cos \xi = \frac{1}{2}\left(1 - \frac{b}{r}\right) + \frac{1}{2}\left(1 + \frac{b}{r}\right)e^{-2\eta}.$$ (7b)

From Eq. (7a), we see that for fixed η, the coordinates (r, z) describe a circle whose radius is $b/\sinh \eta$. If for $\eta = \eta_0$ this circle coincides with the toroidal shell whose minor radius is a, then it is straightforward to show that $b = r_0\left[1 - \left(\frac{a}{r_0}\right)^2\right]^{\frac{1}{2}}$. The points (η, ξ) outside the toroidal shell are determined by the inequality $\eta < \eta_0$, while the points inside the hollow region of the shell are determined by $\eta > \eta_0$. In both regions, the right hand side of Eq. (1) is zero and, in toroidal coordinates, this equation reduces to

$$\frac{1}{h_\eta h_\xi h_\theta}\left[\frac{\partial}{\partial \eta}\left(\frac{h_\xi h_\theta}{h_\eta}\frac{\partial A_\theta}{\partial \eta}\right) + \frac{\partial}{\partial \xi}\left(\frac{h_\theta h_\eta}{h_\xi}\frac{\partial A_\theta}{\partial \xi}\right)\right] - \frac{1}{h_\theta^2}A_\theta = 0,$$ (8)

3

where

$$h_\eta = h_\xi = \frac{b}{\cosh\eta - \cos\xi}, \tag{9a}$$

$$h_\theta = \frac{b\sinh\eta}{\cosh\eta - \cos\xi}. \tag{9b}$$

If we set $A_\theta = b(\cosh - \cos\xi)^{\frac{1}{2}}F(\eta,\xi)$, then the differential equation satisfied by $F(\eta,\xi)$ is a separable equation and its solution can be expressed in terms of the toroidal functions. Specifically, the solutions of Eq. (8) in the two regions inside and outside the toroidal shell are:

$$A_\theta^{in} = b(\cosh\eta - \cos\xi)^{\frac{1}{2}}\sum_{m=0}^{\infty}\epsilon_m a_m(t)Q_{m-\frac{1}{2}}^1(\cosh\eta)\cos m\xi, \tag{10a}$$

$$A_\theta^{out} = A_\theta^{ext} + b(\cosh\eta - \cos\xi)^{\frac{1}{2}}\sum_{m=0}^{\infty}\epsilon_m b_m(t)P_{m-\frac{1}{2}}^1(\cosh\eta)\cos m\xi, \tag{10b}$$

where $\epsilon_0 = 1$, $\epsilon_m = 2$ when $m = 1,2,3,...$, $P_{m-\frac{1}{2}}^1(\cosh\eta)$, $Q_{m-\frac{1}{2}}^1(\cosh\eta)$ are the associated Legendre functions of the first and second kind, respectively, and $A_\theta^{ext}(\eta,\xi,t)$ is the vector potential associated with the applied external field. The time-dependent parameters $a_m(t)$ and $b_m(t)$ are determined from the boundary conditions. Since the ξ-component of the magnetic field is equal to

$$B_\xi = -\frac{1}{h_\eta h_\theta}\frac{\partial}{\partial\eta}h_\theta A_\theta, \tag{11}$$

and the external field is zero at $t = 0$, the boundary conditions of Eqs. (4) and (5), expressed in terms of the vector potential A_θ, become:

$$A_\theta^{in}(\eta_0,\xi,t) = A_\theta^{out}(\eta_0,\xi,t), \tag{12a}$$

$$(\cosh\eta_0 - \cos\xi)^{\frac{3}{2}}\frac{\partial}{\partial\eta}\left(\frac{A_\theta^{out}(\eta,\xi,t) - A_\theta^{in}(\eta,\xi,t)}{(\cosh\eta - \cos\xi)^{\frac{1}{2}}}\right)\Bigg|_{\eta=\eta_0} = -\tau\frac{\partial A_\theta^{in}(\eta_0,\xi,t)}{\partial t} \tag{12b}$$

where $\tau = \mu_0\sigma d_w b$.

In the following, we shall assume that there are no external current coils very near the toroidal conductor or inside it. If η_c is the toroidal coordinate of the coil nearest to the minor axis, and such that $\eta_c < \eta_0$, then the external vector potential A_θ^{ext} is given by

$$A_\theta^{ext} = b(\cosh\eta - \cos\xi)^{\frac{1}{2}}\sum_{m=0}^{\infty}\epsilon_m a_m^{ext}(t)Q_{m-\frac{1}{2}}^1(\cosh\eta)\cos m\xi, \tag{13}$$

for all $\eta > \eta_c$. The time-dependent parameters $a_m^{ext}(t)$ are known and are associated with physical properties of the external field, such as external field index, flux condition, etc.

4

Now, it is straightforward to compute the unknown coefficients a_m, b_m from the boundary conditions. From Eq. (12a) we obtain

$$b_m = \frac{\left(a_m - a_m^{ext}\right) Q_{m-\frac{1}{2}}^1(\cosh \eta_0)}{P_{m-\frac{1}{2}}^1(\cosh \eta_0)}.$$
(14)

Similarly, Eq. (12b) together with Eq. (14) and the identity[6]

$$Q_{m-\frac{1}{2}}^1(u)\frac{dP_{m-\frac{1}{2}}^1(u)}{du} - P_{m-\frac{1}{2}}^1(u)\frac{dQ_{m-\frac{1}{2}}^1(u)}{du} = -\frac{4m^2 - 1}{4(u^2 - 1)},$$
(15)

leads to the following set of coupled differential equations for a_m:

$$\dot{a}_0 = -\frac{1}{\tau_0}\left(a_0 - a_0^{ext}\right) + \frac{1}{\tau_0}\frac{1}{\cosh \eta_0}\frac{Q_{\frac{1}{2}}^1(\cosh \eta_0)}{Q_{-\frac{1}{2}}^1(\cosh \eta_0)}\left(a_1 - a_1^{ext}\right),$$
(16a)

$$\dot{a}_m = -\frac{1}{\tau_m}\left(a_m - a_m^{ext}\right) + \frac{1}{\tau_{m-1}}\frac{1}{2\cosh \eta_0}\frac{Q_{m-\frac{3}{2}}^1(\cosh \eta_0)}{Q_{m-\frac{1}{2}}^1(\cosh \eta_0)}\left(a_{m-1} - a_{m-1}^{ext}\right)$$

$$+ \frac{1}{\tau_{m+1}}\frac{1}{2\cosh \eta_0}\frac{Q_{m+\frac{1}{2}}^1(\cosh \eta_0)}{Q_{m-\frac{1}{2}}^1(\cosh \eta_0)}\left(a_{m+1} - a_{m+1}^{ext}\right),$$
(16b)

where $m = 1, 2, 3, \ldots$ and

$$\tau_m = -\frac{4\tau \tanh \eta_0}{4m^2 - 1}Q_{m-\frac{1}{2}}^1(\cosh \eta_0)P_{m-\frac{1}{2}}^1(\cosh \eta_0).$$
(17)

The toroidal functions $P_{m-\frac{1}{2}}^n$ and $Q_{m-\frac{1}{2}}^n$ appearing in Eqs. (16a), (16b) and (17) are given by the following exact expressions[6]:

$$P_{m-\frac{1}{2}}^n(\cosh \eta) = \frac{2^n\Gamma(m)}{\pi^{\frac{1}{2}}\Gamma(m - n + \frac{1}{2})}(\sinh \eta)^n e^{(m-n-\frac{1}{2})\eta}$$

$$*(1 - \delta_{m0})\sum_{s=0}^{m-1}\frac{(n + \frac{1}{2})_s(n - m + \frac{1}{2})_s}{s!(1 - m)_s}e^{-2s\eta}$$

$$+ \frac{(-1)^n 2^{n+1}\Gamma(m + n + \frac{1}{2})}{\pi^{\frac{3}{2}}\Gamma(m + 1)}(\sinh \eta)^n e^{-(m+n+\frac{1}{2})\eta}\sum_{s=0}^{\infty}\frac{(n + \frac{1}{2})_s(m + n + \frac{1}{2})_s}{s!(m + 1)_s}e^{-2s\eta}$$

$$*\left[\ell n(4e^\eta) + u_s + u_{m+s} - v_{n+s} - v_{m+n+s}\right],$$
(18a)

5

$$Q_{m-\frac{1}{2}}^n(\cosh\eta) = \frac{(-1)^n 2^n \Gamma(m+n+\frac{1}{2})}{\Gamma(m+1)}(\sinh\eta)^n e^{-(m+n+\frac{1}{2})\eta}$$

$$* \sum_{s=0}^{\infty} \frac{(n+\frac{1}{2})_s (m+n+\frac{1}{2})_s}{s!(m+1)_s} e^{-2s\eta}, \tag{18b}$$

where

$$(a)_s = a(a+1)(a+2)...(a+s-1), \qquad (a)_0 = 1, \tag{19a}$$

$$u_n = \frac{1}{2}\sum_{k=1}^{n}\frac{1}{k}, \qquad u_0 = 0, \tag{19b}$$

$$v_n = \sum_{k=1}^{n}\frac{1}{2k-1}, \qquad v_0 = 0. \tag{19c}$$

For $m = 0$, the first term in Eq. (18a) is omitted, since $\delta_{mn} = 1$ for $m = n$, and $\delta_{mn} = 0$ for $m \neq n$. The expressions above are appropriate for the region inside the toroidal conductor, i.e., for $\eta > \eta_0$, as well as on its surface.

Up to this point the results are exact. For small aspect ratio $a/r_0, e^{-\eta_0} = (r_0 + a - b)/(r_0 + a + b) \approx a/2r_0 << 1$. Thus, to the lowest order in the aspect ratio, Eq. (17) becomes

$$\tau_0 = 2\tau_D\left[\ell n\frac{8r_0}{a} - 2\right], \tag{20a}$$

$$\tau_m = \frac{\tau_D}{m}, \tag{20b}$$

where $m = 1, 2, 3, ...$, and

$$\tau_D = \frac{\mu_0\sigma d_w a}{2}. \tag{21}$$

The time τ_0 is the L/R time of the toroidal conductor, while τ_m are the higher order diffusion times.

An approximate expression for A_θ^{in} can be obtained from Eq. (10a) by keeping terms up to order $e^{-2\eta}$, i.e., up to second order toroidal corrections. Making use of the identity[6]

$$(\cosh\eta - \cos\xi)^{\frac{1}{2}} = \sum_{m=0}^{\infty}\epsilon_m C_m(\eta)\cos m\xi, \tag{22}$$

where

$$C_0(\eta) = \frac{\sqrt{2}}{2\pi}e^\eta\left(1 + e^{-2\eta}\right)\left[Q_{-\frac{1}{2}}(\cosh\eta) - \frac{2e^{-\eta}}{1 + e^{-2\eta}}Q_{\frac{1}{2}}(\cosh\eta)\right], \tag{23a}$$

$$C_m(\eta) = \frac{\sqrt{2}}{2\pi}e^\eta(1 + e^{-2\eta}) \tag{23b}$$

6

$$* \left[Q_{m-\frac{1}{2}}(\cosh \eta) - \frac{e^{-\eta}}{1 + e^{-2\eta}} \left(Q_{m-\frac{3}{2}}(\cosh \eta) + Q_{m+\frac{1}{2}}(\cosh \eta) \right) \right],$$

and also of Eq. (18b), a lengthy calculation leads to the approximate expression

$$A_\theta^{in} \approx -\frac{\pi}{2\sqrt{2}} b \left[a_0 + \frac{3}{2}(a_0 - a_1)e^{-2\eta} \right. \tag{24}$$

$$\left. -(a_0 - 3a_1)e^{-\eta} \cos \xi - \frac{1}{4}(a_0 + 6a_1 - 15a_2)e^{-2\eta} \cos 2\xi \right].$$

Using Eqs. (7a), (7b) and keeping terms up to order $\left(1 - \frac{b}{r}\right)^2$ and $(z/r)^2$, Eq. (24) reduces to

$$A_\theta^{in} \approx -\frac{\pi}{2\sqrt{2}} b \left[a_0 - \frac{1}{2}(a_0 - 3a_1)(1 - \frac{b}{r}) \right. \tag{25}$$

$$\left. + \frac{1}{16}(a_0 + 15a_2)(1 - \frac{b}{r})^2 + \frac{3}{16}(a_0 + 4a_1 - 5a_2)(\frac{z}{r})^2 \right],$$

i.e., the approximate A_θ^{in} has been expressed in terms of the cylindrical coordinates (r, z). The magnetic field components near the minor axis are determined from Eqs. (2a) and (2b) and are equal to

$$B_r^{in} \approx -B_{z0} n_D \frac{z}{r}, \tag{26a}$$

$$B_z^{in} \approx B_{z0} \left[1 - n_D(1 - \frac{b}{r}) \right], \tag{26b}$$

where

$$B_{z0} = -\frac{\pi}{4\sqrt{2}}(a_0 + 3a_1), \tag{27a}$$

is the vertical field component near the minor axis and

$$n_D = \frac{3}{4} \frac{a_0 + 4a_1 - 5a_2}{a_0 + 3a_1}, \tag{27b}$$

is the field index. To first order in a/r_0, the magnetic flux Φ_0 through the area πr_0^2 on the midplane is

$$\Phi_0 = 2\pi r_0 A_\theta^{in}(r_0, 0, t) \tag{28}$$

$$\approx -2\pi r_0^2 \frac{\pi}{2\sqrt{2}} a_0$$

Defining ϵ_D by means of the relation $\Phi_0 \equiv 2\pi r_0^2 B_{z0}(1 - \epsilon_D)$, the vertical component of the field on the minor axis can be written

$$B_{z0}(1 - \epsilon_D) = -\frac{\pi}{2\sqrt{2}} a_0. \tag{29}$$

The parameter ϵ_D is a measure of the flux condition. When $\epsilon_D = 0$, the betatron flux condition is satisfied.

The quantities a_0, a_1, a_2 are determined completely by the magnetic field, the field index and the flux on the minor axis, and, therefore, are parametric representations of these physical quantities. But the vector potential that describes the external field in Eq. (13) has exactly the same form as A_θ^{in} in Eq. (10a). Therefore, if B_0, n and $\Phi_0^{ext} = 2\pi r_0^2 B_0(1 - \epsilon)$ are the external field, external field index and external flux on the minor axis, then a_0^{ext}, a_1^{ext} and a_2^{ext} can be expressed as follows:

$$a_0^{ext} = -\frac{2\sqrt{2}}{\pi} B_0(1 - \epsilon), \tag{30a}$$

$$a_1^{ext} = -\frac{2\sqrt{2}}{3\pi} B_0(1 + \epsilon), \tag{30b}$$

$$a_2^{ext} = -\frac{2\sqrt{2}}{15\pi} B_0(7 - 8n + \epsilon). \tag{30c}$$

These expressions are used in solving Eqs. (16a), (16b). It is assumed that only B_0 is time-dependent. This is a valid assumption provided that the coils that generate the external field, carry the same current and are filaments, i.e., there is no diffusion process associated with them.

All the physical quantities of interest have been computed to first order in toroidal corrections. Therefore, it is sufficient to compute the parameters a_0, a_1, a_2 to first order in a/r_0. If all terms of order $e^{-2\eta_0}$ or higher are omitted, Eqs. (16a), (16b) become

$$\dot{a}_0 \approx -\frac{1}{\tau_0}(a_0 - a_0^{ext}), \tag{31a}$$

$$\dot{a}_m \approx -\frac{1}{\tau_m}(a_m - a_m^{ext}) + \frac{1}{\tau_{m-1}}\frac{2m}{2m+1}(a_{m-1} - a_{m-1}^{ext}), \tag{31b}$$

where $m = 1, 2$. This system of equations can be integrated easily. Under the initial conditions $a_m(0) = 0$, the solutions for $\tau_2 = \tau_1/2$ are:

$$a_0 = -\frac{2\sqrt{2}}{\pi}(1 - \epsilon)A_0, \tag{32a}$$

$$a_1 = -\frac{2\sqrt{2}}{3\pi}\left[\left(1 + \epsilon - \frac{2\alpha}{1-\alpha}(1 - \epsilon)\right)A_1 + \frac{2\alpha}{1-\alpha}(1 - \epsilon)A_0\right], \tag{32b}$$

$$a_2 = -\frac{2\sqrt{2}}{15\pi}\left[\left(7 - 8n + \epsilon - 4(1 + \epsilon) + \frac{8\alpha}{2-\alpha}(1 - \epsilon)\right)A_2\right.$$

$$+ \left(4(1 + \epsilon) - \frac{8\alpha}{1 - \alpha}(1 - \epsilon) \right) A_1 + \frac{8\alpha}{(1 - \alpha)(2 - \alpha)}(1 - \epsilon)A_0 \Bigg] , \tag{32c}$$

where

$$\alpha = \frac{\tau_1}{\tau_0}, \tag{33a}$$

and

$$A_m = \frac{1}{\tau_m} e^{-t/\tau_m} \int_0^t e^{t'/\tau_m} B_0(t') dt'. \tag{33b}$$

Substitution of a_0, a_1, a_2 into Eqs. (27a), (27b) leads to

$$B_{z0} = \left(\frac{1}{2} + \frac{\alpha}{1 - \alpha} \right) (1 - \epsilon)A_0 + \left[1 - \left(\frac{1}{2} + \frac{\alpha}{1 - \alpha} \right) (1 - \epsilon) \right] A_1, \tag{34a}$$

$$n_D = \frac{\left(\frac{3}{8} + \frac{\alpha}{2 - \alpha} \right) (1 - \epsilon)A_0 + \left[n - \left(\frac{3}{8} + \frac{\alpha}{2 - \alpha} \right) (1 - \epsilon) \right] A_2}{\left(\frac{1}{2} + \frac{\alpha}{1 - \alpha} \right) (1 - \epsilon)A_0 + \left[1 - \left(\frac{1}{2} + \frac{\alpha}{1 - \alpha} \right) (1 - \epsilon) \right] A_1}. \tag{34b}$$

Another interesting physical quantity is the surface wall current density, which is given by

$$J_{s\theta} = -\sigma d_w \frac{\partial A_\theta^{in}(\eta_0, \xi, t)}{\partial t}. \tag{35}$$

To first order in toroidal corrections, Eqs. (25), (31a), (31b), (32a), (32b) give

$$J_{s\theta} \approx \frac{2r_0}{\mu_0 a} \left\{ \alpha(1 - \epsilon)(A_0 - B_0) - \left[\left(4 + \alpha - \frac{2\alpha}{1 - \alpha} \right) (1 - \epsilon)(A_0 - B_0) \right. \right. \tag{36}$$

$$\left. \left. - \left(1 + \epsilon - \frac{2\alpha}{1 - \alpha}(1 - \epsilon) \right) (A_1 - B_0) \right] \frac{a}{r_0} \cos \phi \right\} ,$$

where $\cos \phi = (r - r_0)/a$ and r is the radial position of any point on the wall chamber. The wall current is equal to

$$I = \int_0^{2\pi} J_{s\theta} a d\phi \tag{37}$$

$$= \frac{4\pi r_0}{\mu_0} \alpha(1 - \epsilon)(A_0 - B_0).$$

As a first application, consider a rising external magnetic field that reaches a constant value, i.e.,

$$B_0(t) = b_0(1 - e^{-t/\tau_{ext}}). \tag{38}$$

From Eq. (33b), we have:

$$A_m = b_0 \left[1 - \frac{1}{1 - \frac{\tau_m}{\tau_{ext}}} e^{-t/\tau_{ext}} + \frac{\tau_m/\tau_{ext}}{1 - \frac{\tau_m}{\tau_{ext}}} e^{-t/\tau_m} \right]. \tag{39}$$

For $t \gg \tau_{ext}$ and $t \gg \tau_m$, the coefficient $A_m \approx b_0$ and from Eqs. (34a), (34b), $B_{z0} \approx b_0$ and $n_D \approx n$. Also the wall current goes to zero. All three conclusions are as expected.

For a sinusoidally varying field

$$B_0(t) = b_0 \sin \omega t, \tag{40}$$

the coefficients A_m are given by

$$A_m = \frac{b_0}{1 + (\omega \tau_m)^2} \left[\sin \omega t - \omega \tau_m \cos \omega t + \omega \tau_m e^{-t/\tau_m} \right] \tag{41}$$

After a long time, i.e., for $t \gg \tau_m$, the external field and the field on the minor axis are not in phase, but their phase difference remains constant. On the other hand, for small times, i.e., for $\omega t \ll 1$ and $t \ll \tau_m$, the coefficients $A_m \approx b_0 \omega t^2 / 2\tau_m$ and the field index becomes

$$n_D(t = 0) = \frac{16n - (5\alpha + 6)(1 - \epsilon)}{4[2 - (1 + \alpha)(1 - \epsilon)]}. \tag{42}$$

Furthermore, assuming that $\omega \tau_m \ll 1$ and $\omega t \ll 1$, but not $t \gg \tau_m$, we obtain

$$A_m \approx b_0 \omega \left[t - \tau_m (1 - e^{-t/\tau_m}) \right], \tag{43}$$

and

$$B_{z0} \approx b_0 \left[t - \tau_d + \frac{\tau_d - \tau_1}{\tau_0 - \tau_1} \tau_0 e^{-t/\tau_0} - \frac{\tau_d - \tau_0}{\tau_0 - \tau_1} \tau_1 e^{-t/\tau_1} \right], \tag{44}$$

where the delay time τ_d is equal to

$$\tau_d = \frac{(1 - \epsilon)\tau_0 + (3 - \epsilon)\tau_1}{2}. \tag{45}$$

In contrast, the delay time for a cylinder of infinite length is equal to the diffusion time. It is apparent from Eq. (45) that in the case of the toroidal conducting shell, the delay time depends linearly on both the L/R time τ_0 and the diffusion time τ_1. In addition, for a toroidal shell, B_{z0} has an exponentially decreasing dependence on both times τ_0 and τ_1, while the wall current, from Eq. (37), depends only upon τ_0, i.e.,

$$I = -\frac{4\pi \tau_0}{\mu_0} \omega \tau_1 b_0 (1 - \epsilon) \left(1 - e^{-t/\tau_0} \right), \tag{46}$$

i.e., it reaches exponentially its maximum value with the L/R time τ_0.

A direct comparison has been made between the theory presented above and the numerical results from the 2-dimensional TRIDIF code. The set of parameters used for

the comparison are listed in Table I. For these parameters, Eqs. (20a), (20b), (45), give $\tau_0 = 11.28$ μsec, $\tau_1 = 2.95$ μsec, $\alpha = 0.26$, and $\tau_d = 10.42$ μsec. The solid curves in Figs. 2(a)-2(d) show B_{z0}, n_D, $\Phi_0/(\pi r_0^2 B_{z0})$, and I as a function of time . In the computer run, the inner minor radius of the toroidal conductor is 15 cm and the outer minor radius is 17 cm. In the region of the chamber, the mesh has a cell size $\Delta r = 0.5$ cm, $\Delta z = 1.0$ cm, but further out it is much less dense. Thus, in the radial direction there are 157 mesh points over a distance of 300 cm, while in the vertical direction there are 71 mesh points over a distance of 200 cm, and the time step used is $\Delta t = 0.5$ μsec. Advantage is taken of the midplane symmetry, i.e., the calculation is confined to the region $z \geq 0$. The external field is generated by current filaments (coils) located at the same positions as in the modified betatron experiment. All the coils carry the same current and have the same sinusoidal dependence. In the absence of the toroidal chamber the maximum vertical field generated by these coils on the minor axis, i.e., at $r = 100$ cm, $z = 0$, is $B_0 = 1267$ Gauss, when the maximum current through the coils is 40 kA. This is the value of b_0 used in the theory. In the absence of the toroidal chamber, these coils generate a field index of 0.54 on the minor axis and an $\epsilon = -0.067$, but the values chosen in the theory are slightly different, so that at times $t > 30$ μsec the theoretical and numerical n_D and $\Phi_0/(\pi r_0^2 B_{z0})$ are identical.

The dashed curves in Figures 2(a) – 2(d) give the predictions of the code for B_{z0}, n_D, $\Phi_0/(\pi r_0^2 B_{z0})$ and I as a function of time. The straight line in Fig. 2(a) is B_{z0}, when $\sigma = 0$. The numerical delay time, obtained from Fig. (2a), is 9.7 μsec as compared to the theoretical value of 10.42 μsec. The small difference is attributed to the fact that τ_0 and τ_1 depend on the volume of the numerical integration. It should be noticed that in the numerical calculation the integration has been carried inside a cylinder of radius 300 cm and of half-height 200 cm, while in the theoretical work the integration has been carried out over the whole space. To obtain some insight into this effect, let us look at the diffusion through a cylindrical conducting shell of infinite length, where the region of the numerical integration is limited within a perfect conductor located at a radius r_1. The diffusion time is equal to $\tau_D \left[1 - (a/r_1)^2\right]$, where a is the radius of the conductor and τ_D is given by Eq. (21). It is apparent that the diffusion time decreases as the volume of the integration region decreases, and, therefore, the inductance of the system decreases. As another example consider a toroidal conducting shell, with a region of integration confined within a perfect conductor located at $\eta = \eta_1$ and therefore the radial positions r are limited to the values between $r_{1\ min} = b\tanh(\eta_1/2)$ and $r_{1\ max} = b\coth(\eta_1/2)$. All the theoretical results obtained above remain the same except for the L/R time in Eq. (20a)

11

that is replaced by $2\tau_D \left[\ell n \dfrac{8r_0}{a} - 2 - \left(\dfrac{\pi r_0}{2r_{1\,max}}\right)^2\right]$. Again, the L/R time (but not the times τ_1, τ_2) decreases as the volume of the integration region decreases and so does τ_d. In the example given above the region for $r < r_{1min}$ is excluded, while in the numerical results this region is included. For this reason, the comparison of the numerical results is made with the theoretical results for the whole space rather than a finite region of integration. The largest discrepancy between theory and numerical computation is in the field index for small times. This could be due to the large time step (0.5 μsec) that was used in the numerical integration or to the fact that the field index is computed from the second derivative of the stream function rA_θ and this function is not accurately computed initially by the code. The same argument is applicable to the smaller discrepancy, for short times, in the quantity $\Phi_0/(\pi r_0^2 B_{z0})$. Over all, however, the agreement is fairly good between theory and numerical computation with the TRIDIF code.

III. Experimental Results

This section briefly summarizes the measurements on the time delay of the vertical magnetic field caused by the vacuum chamber of the device and compares the experimental results with the predictions of the theory and that of the computer code.

The NRL modified betatron comprises three different external magnetic fields; the betatron field that is a function of time and is responsible for the acceleration of the electrons, the toroidal magnetic field that varies only slightly during the acceleration of the electron ring and the strong focusing field that also has a very weak time dependence. These three fields have been described previously. However, for completeness we briefly describe in this paper the vertical field and the vacuum chamber.

The betatron magnetic field controls mainly the major radius of the gyrating electron ring and is produced by a set of 18 air core (see Fig. 3), circular coils connected in series. Sixteen main coils and four trimmers are used to generate a field configuration with a flux condition equal to 1.92. Their total inductance is approximately 343 μH. The coils are powered by an 8.64 mF capacitor bank that can be charged up to 17 kV. At full charge, the bank delivers to the coils a peak current of about 45 kA. The current flowing through the coils produces a sinusoidally varying field having a quarter period of 2.6 msec and its amplitude on the minor axis at peak charging voltage is 2.1 kG. Immediately after the peak the field is crowbarred with a 4.5 msec decay time. The temporal profile of the vertical field is shown in Fig. 4.

12

The flux condition and field index are adjusted by two sets of trimmers that are connected in parallel to the main coils. The current through the trimmers is adjusted with series inductors. Typically 10 – 15% of the total current flows through the trimmers.

The 100 cm major radius, 15.2 cm inside minor radius vacuum chamber has been constructed using epoxy reinforced carbon fibers. The desired conductivity is obtained by embedding a phosphor bronze screen inside the body of the graphite as shown in Fig. 5. The graphite is 2.5 mm thick and has a surface resitivity of 26.6 mΩ on a square. The screen has 250×250 wires per inch and is made of 40 μm diameter wire with an equivalent surface resistivity of 12.8 mΩ on a square. The calculated resistance for the entire vacuum chamber is 57 mΩ. The measured D.C. resistance of the toroidal vacuum vessel is 68 ± 2 mΩ. The outside surface of the chamber is covered with a 6.3 mm thick, epoxy reinforced fiberglas layer. Figure 6 is a photograph of the vacuum chamber.

This novel construction technique has several attractive features, including controllable resistivity and thus magnetic field penetration time, high stiffness and tensile strength, high radiation resistance (up to 500 Mrad) and low outgassing rate ($\sim 10^{-8}$ Torr/sec-cm^2).

The vertical magnetic field is monitored with a small magnetic probe that is located on the minor axis. The probe has been wound of gauge 35 copper wire, it has approximately 600 turns, its measured inductance is 6.2 mH and its measured internal resistance is 43 Ω. The output of the probe is fed to a passive integrator with a time constant of 20.5 msec.

To improve the time response of the probe the 50Ω terminator at the input of the integrator has been omitted. Oscillations in the output signal have been avoided by locating the oscilloscope approximately 2 m away from the probe, inside an aluminum housing cladded with mu metal.

Results from the measurements are shown in Fig. 7. The lower trace is the output of the probe when it is located inside the vacuum chamber and the upper trace is the output of the probe after the chamber is removed (vacuum field). It is apparent from the oscillogram that after approximately 60 μsec the two signals are parallel and the lower is delayed from the upper by 34 μsec.

For the parameters of the vacuum chamber, and when the flux condition $\phi_0 / \pi r_0^2 B_{z0}$ is equal to 1.92, i.e., for $\epsilon = 0.04$ both theory and the computer code predict a time delay of 37 μsec. The less than 10% difference between the two delay times is probably within the uncertainty of the measurement.

In addition, we broke the electrical continuity of the vacuum chamber by unbolting the joint of two adjacent sectors. The probe was placed on the minor axis with its axis of

13

symmetry on the vertical plane that passes through the symmetry plane of the gap. The intermediate trace in Fig. 7 shows the output of the probe for this measurement.

It is expected that at the symmetry plane of the gap the magnetic field to be identical to the vacuum field. However, due to various constraints, the diameter of the probe and the gap width are approximately equal and thus the measured field is lower than the vacuum field.

IV. Conclusion

The diffusion of the magnetic field through a toroidal conducting shell has been studied under the assumption of a small aspect ratio. The external magnetic field can have an arbitrary field index and magnetic flux on the minor axis of the torus. The diffused field, field index, magnetic flux and wall current were computed analytically and compared with the numerical results from the TRIDIF code. Three time constants determine the evolution in time of the diffusion process, namely, the L/R time τ_0, the diffusion time τ_1, and $\tau_2 = \tau_1/2$. The delay time depends linearly on τ_0, τ_1 and also on the flux condition of the external field. The analytic delay time was larger to that computed from the TRIDIF code. The difference is attributed to the finite volume of the region of integration in the numerical computation which causes the inductance of the system to be smaller. In general, the agreement between the theoretical and numerical results is quite good.

A measurement of the delay time in the toroidal chamber of the NRL modified betatron gave a delay time approximately equal to 34 μsec, i.e., less than 10% smaller from the theoretical value of 37 μsec.

In conclusion, we have seen that the diffusion process in the toroidal conducting shell is much more complicated than that in a conducting cylinder. Therefore, the results for a cylinder cannot be generalized to apply to a toroidal device. The case of the torus should be investigated on its own merit.

Table I.

Parameters for the diffusion theory.

Torus major radius, r_0 (cm)	100
Torus minor radius, a (cm)	16
Chamber wall thickness, d_w (cm)	2
Torus wall conductivity, σ (mho/cm)	14.666
Amplitude of sinusoidal external magnetic field, b_0 (Gauss)	1267
Period of external magnetic field, T (μsec)	10^4
Field index of external magnetic field, n	0.53
Flux condition parameter of external magnetic field, ϵ	-0.05

References

[1] J.C. Jaeger, Phil. Mag. **29**, 18 (1940).

[2] C.A. Kapetanakos, University of Maryland, Department of Physics and Astronomy Technical Report No. 70-113, June 1970.

[3] H. Knoepfel, Pulsed High Magnetic Fields (North-Holland Publishing Co., Amsterdam, 1970).

[4] P. Rolicz, J. Purczynski, and R. Sikora, J. Appl. Phys. **47**, 4127 (1976).

[5] J.R. Freeman, J. Comput. Phys. **41**, 142 (1981).

[6] A. Erderlyi, Higher Transcendental Functions (McGraw-Hill, New York, 1953), Vol. 1.
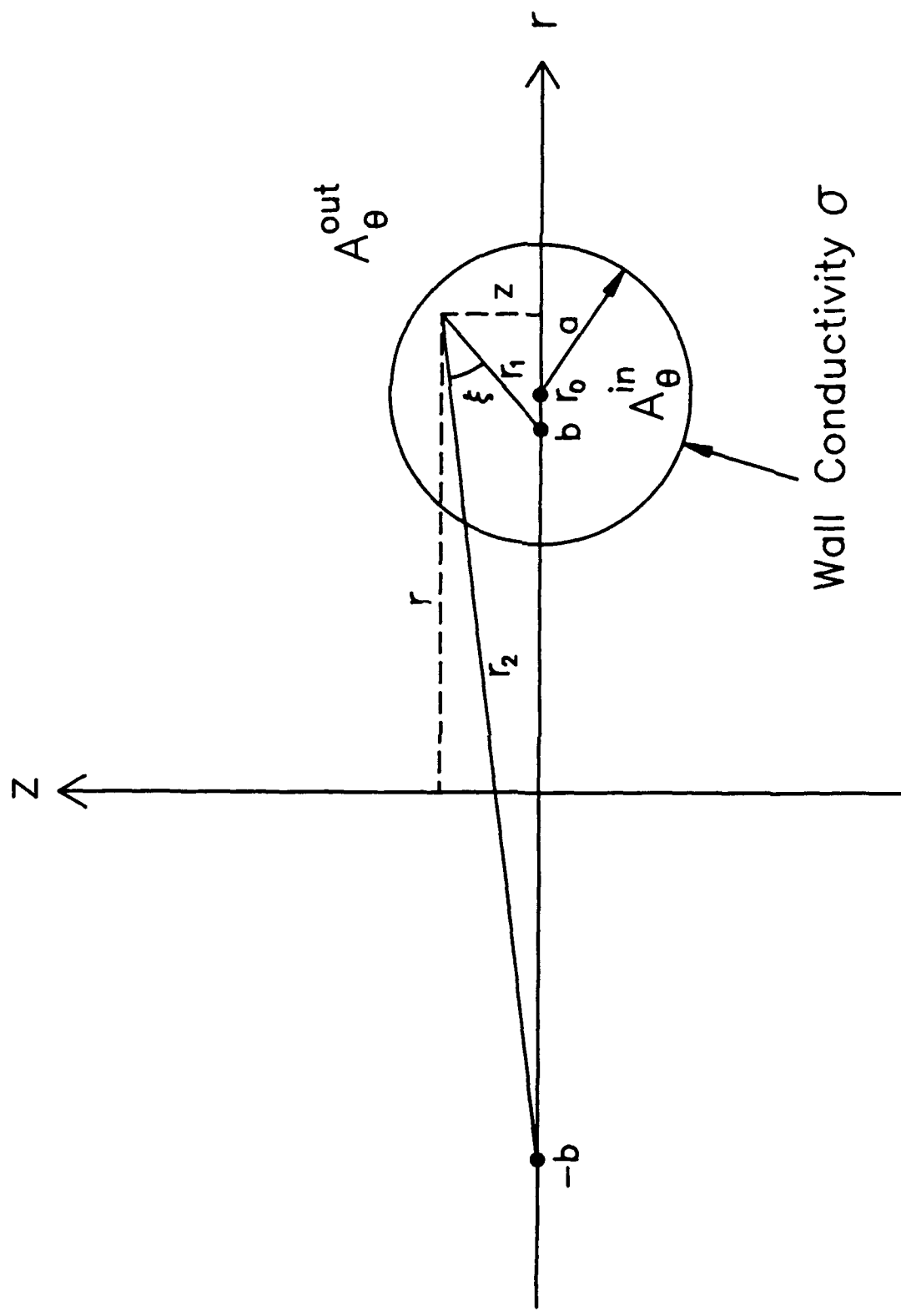
Fig. 1 — Toroidal shell and coordinate systems used in the analysis

17
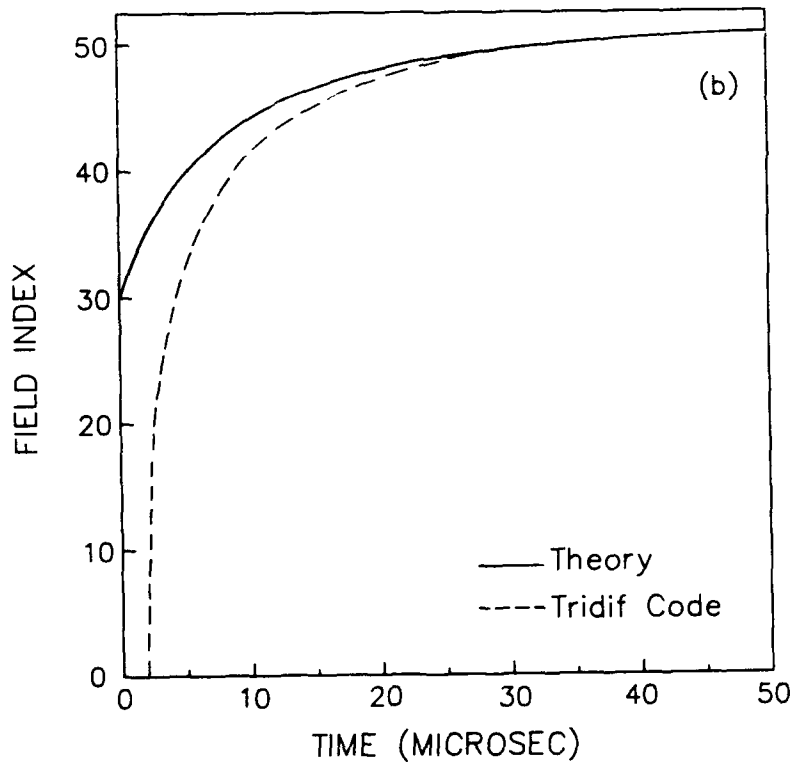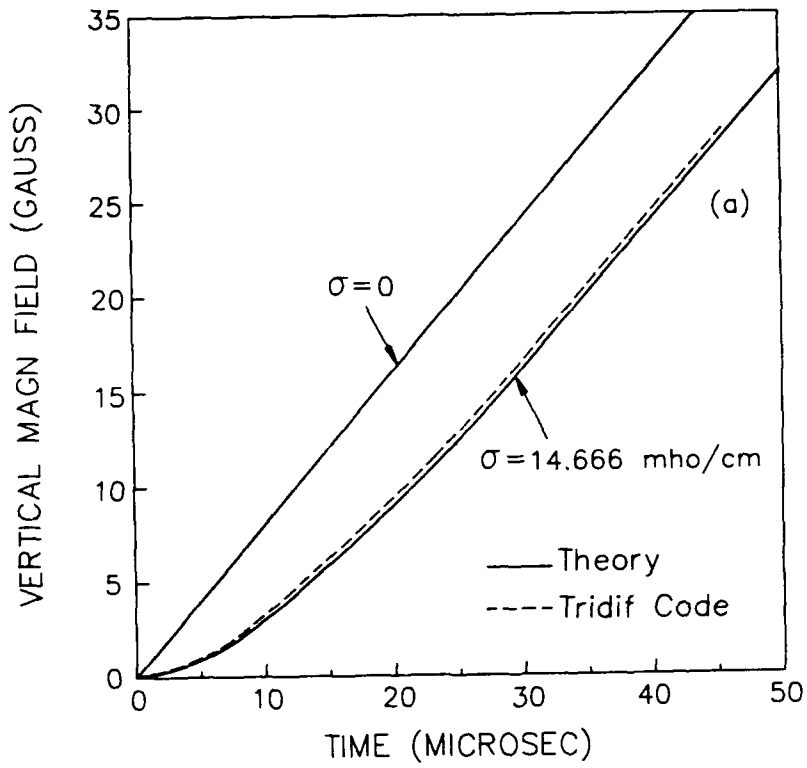
Fig. 2 — Temporal profiles from analysis (solid line) and computer code (dashed line). (a) vertical (betatron) field, (b) field index, (c) flux condition, and (d) wall current.
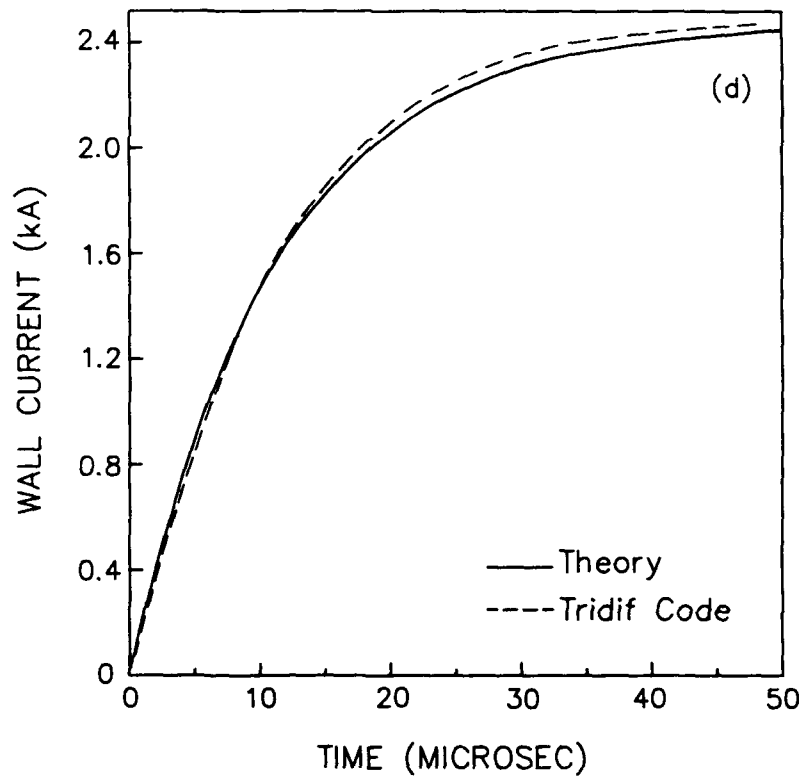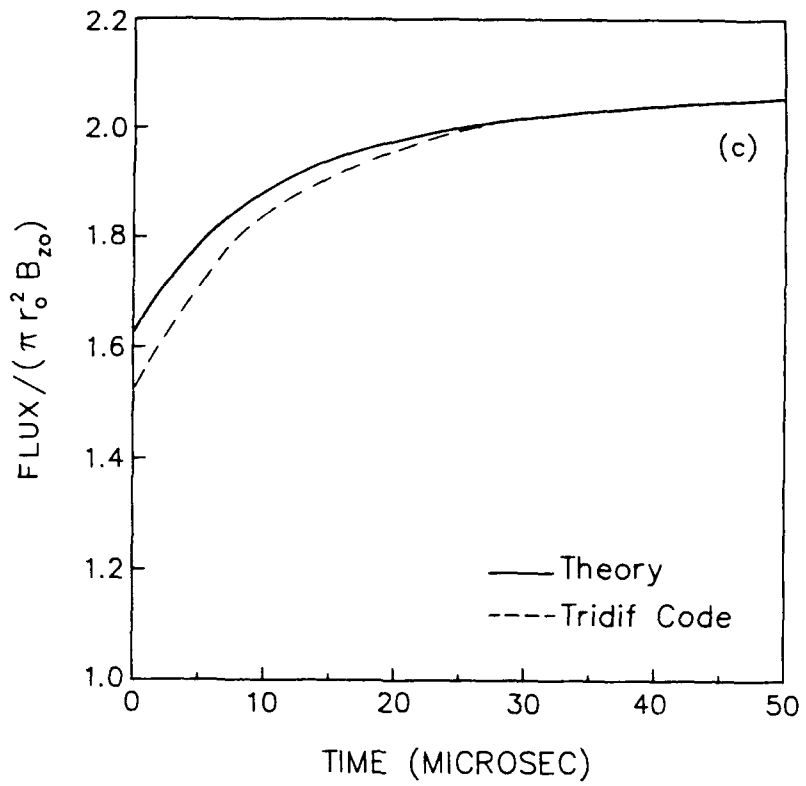
Fig. 2 — (continued) Temporal profiles from analysis of the (solid line) and computer code (dashed line). (a) vertical (betatron) field, (b) field index, (c) flux condition, and (d) wall current.
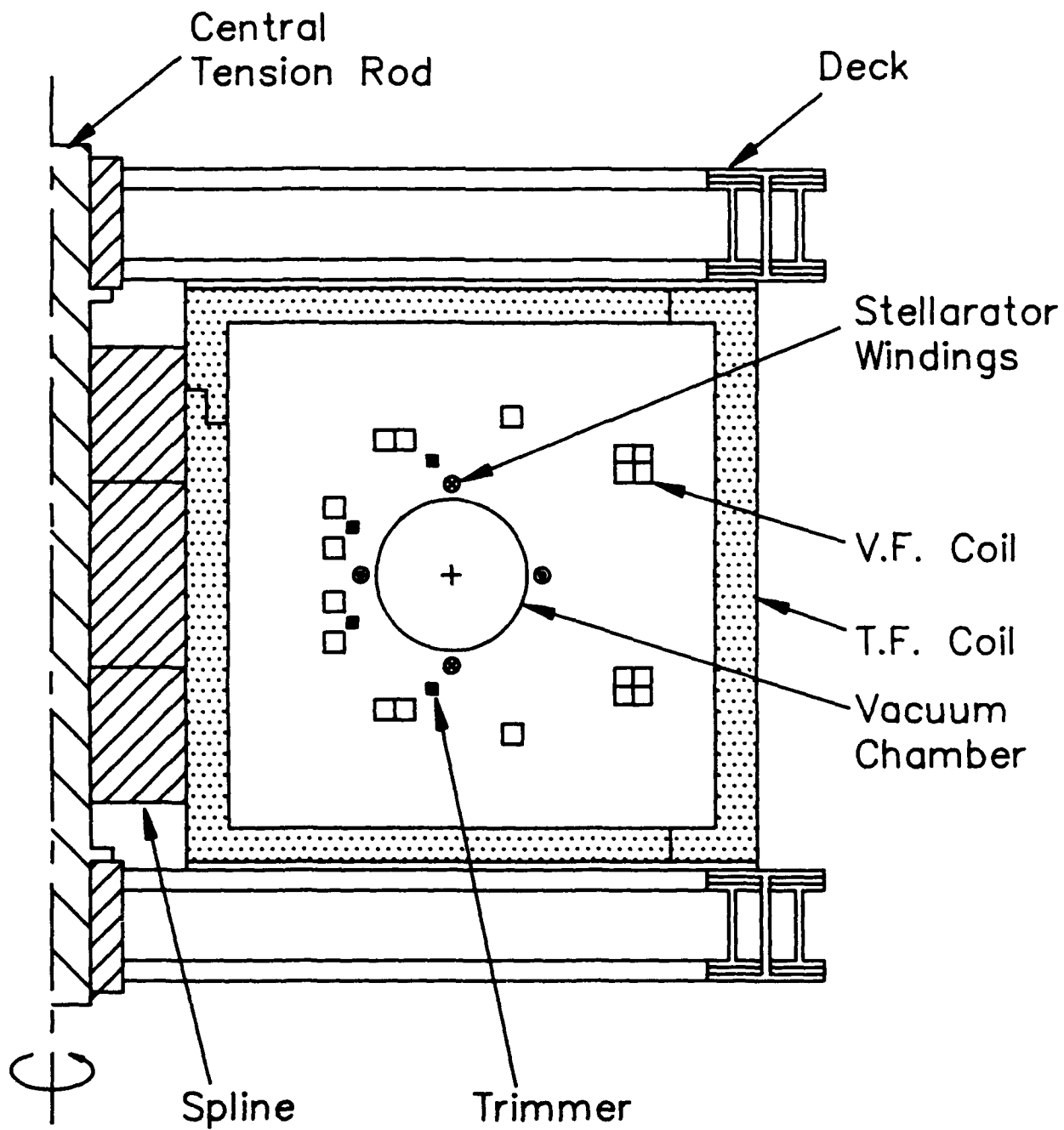
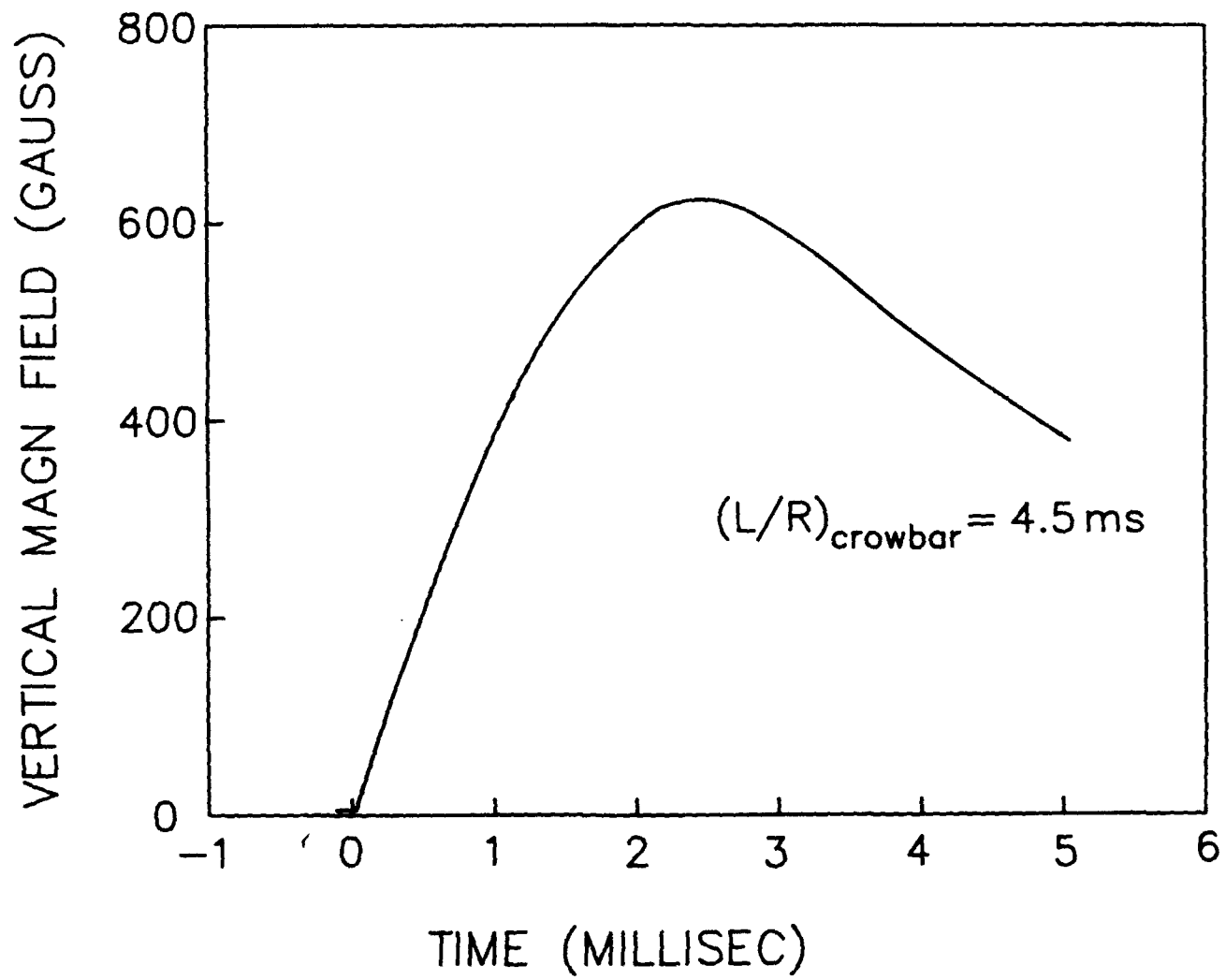Fig. 3 — Elevation of the experiment

Fig. 4 — Vertical (betatron) field vs. time

VACUUM CHAMBER WALL COMPOSITION

See Detail A

30° Sector of Chamber

100 cm Major Radius

15 cm Minor Radius

Graphite Reinforced
Low Outgassing Epoxy

Vacuum
Surface

1/8"

1/4"

Fiberglass Reinforced
Low Outgass Epoxy

Phospher Bronze Screen

Atmosphere

$(250 \times 250 \, \frac{Wires}{Inch}, \, 1.6 \, mil \, wire)$
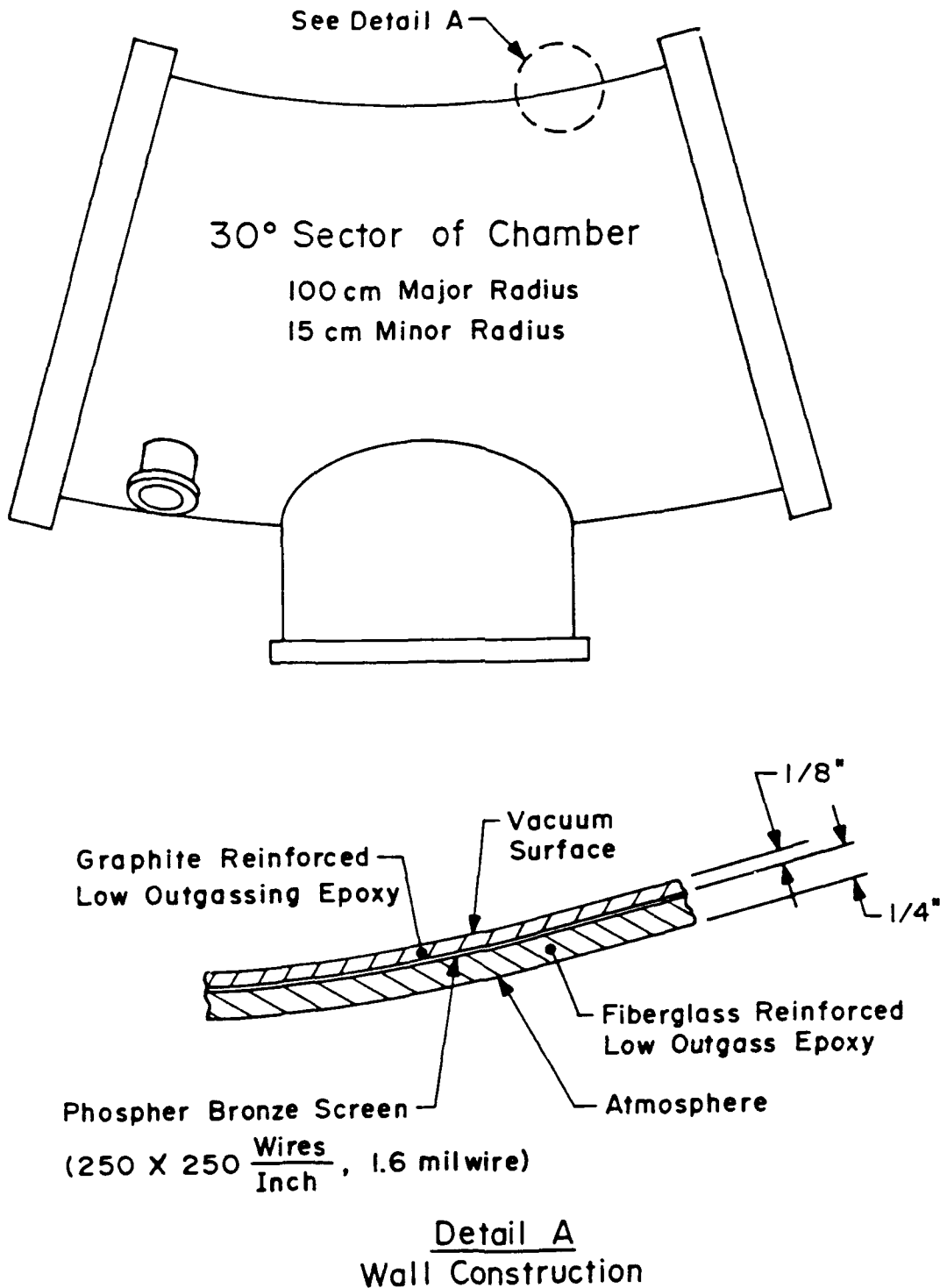
Detail A
Wall Construction

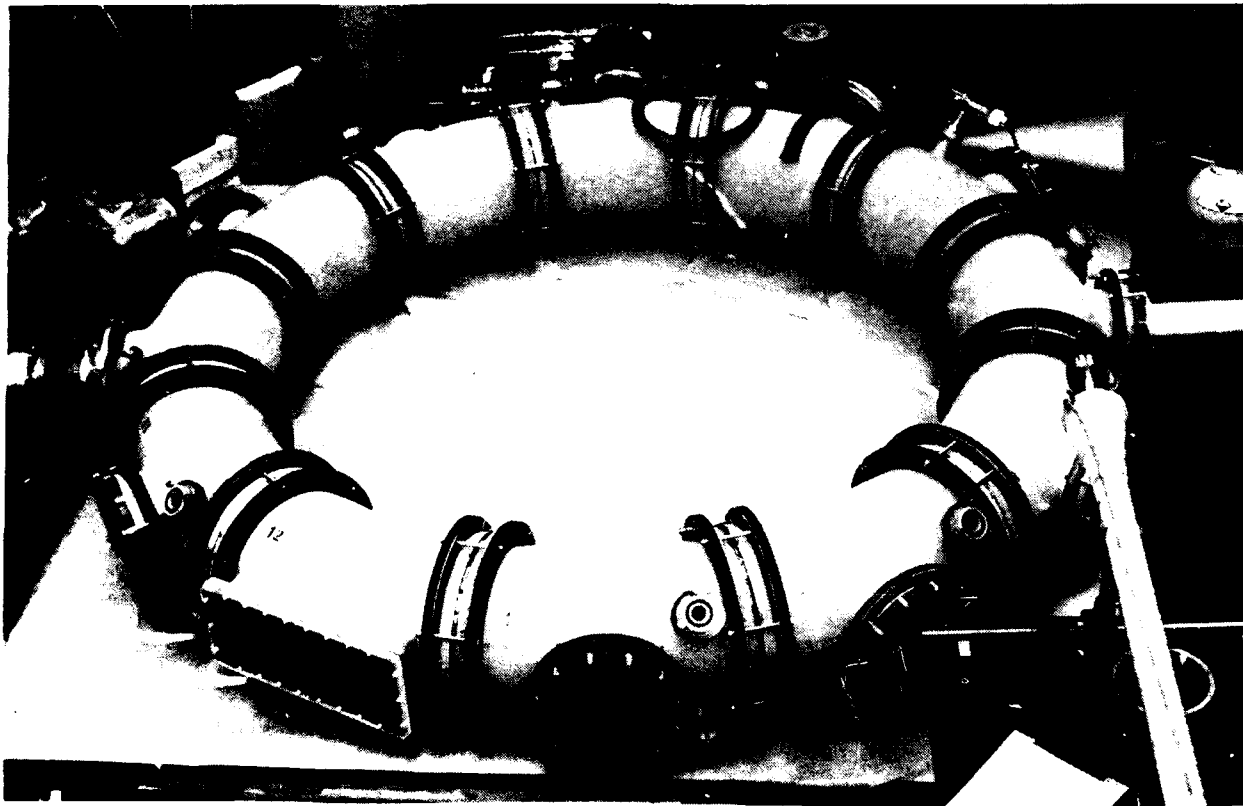Fig. 5 — 30° sector of the vacuum chamber and details of wall construction

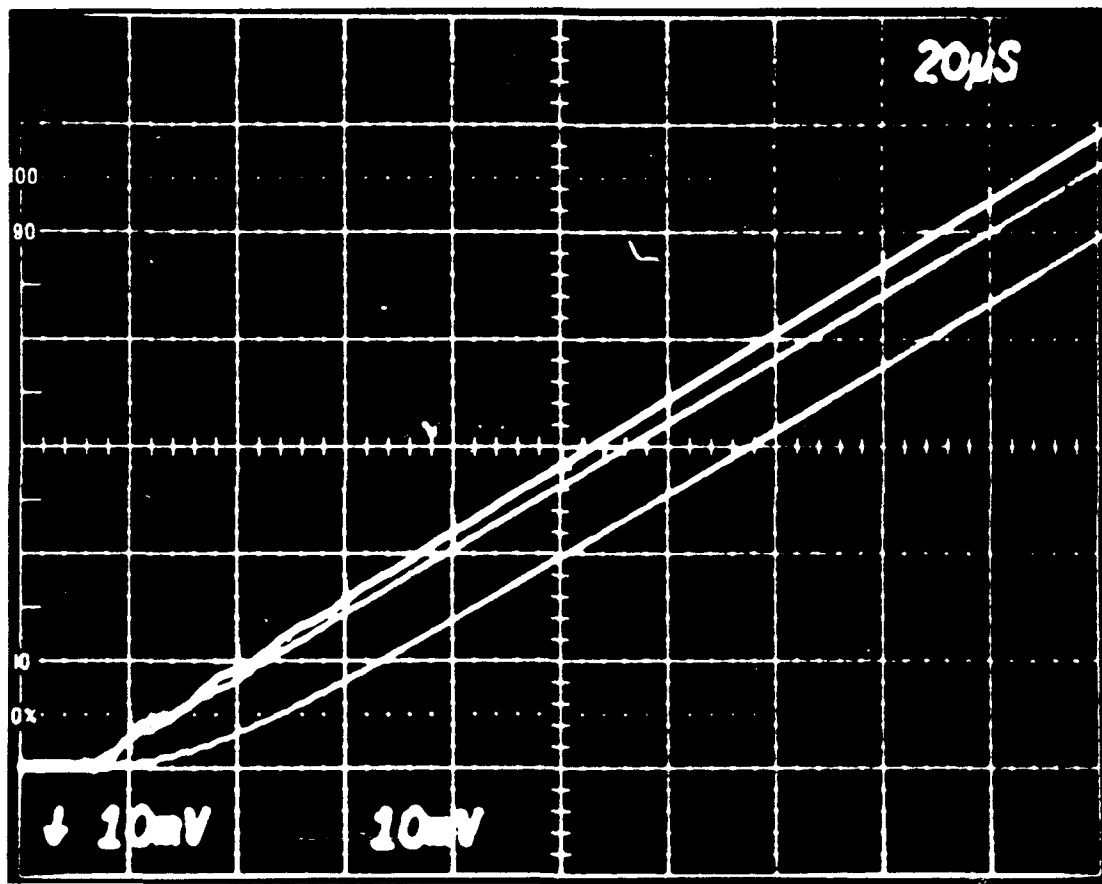Fig. 6 — Photograph of the epoxy reinforced-carbon fiber vacuum chamber

Fig 7 Measured vertical magnetic field vs. time of the minor axis (r = 100 cm., z = 0) of the torus. Bottom trace: Inside the complete vacuum chamber with a gap. Top trace: After the removal of the chamber (vacuum field).

Dr. M. Allen
Stanford Linear Accelerator Center
Stanford, CA 94305

Dr. W. Barletta
Lawrence Livermore National Laboratory
P.O. Box 808
Livermore, CA 94550

Dr. M. Barton
Brookhaven National Laboratory
Upton, L.I., NY 11101

Dr. Jim Benford
Physics International Co.
2700 Merced St.
San Leandro, CA 94577

Dr. Kenneth Bergerson
Plasma Theory Division - 5241
Sandia National Laboratories
Albuquerque, NM 87115

Dr. Daniel Birx
Lawrence Livermore National Laboratory
P.O. Box 808
Livermore, CA 94550

Dr. Charles Brau
Los Alamos Scientific Laboratory
Los Alamos, NM 87544

Dr. R. Briggs
SSC Lab
Stoneridge Office Park
2550 Beckleymeade Ave. Ste 260
Dallas, TX 75237

Dr. Allan Bromborsky
Harry Diamond Laboratory
2800 Powder Mill Road
Adelphi, MD 20783

Dr. H. Lee Buchanan
DARPA
1400 Wilson Blvd.
Arlington, VA 22209-2308

Dr. M. Butram
Sandia National Laboratory
Albuquerque, NM 87115

Dr. M. Caponi
TRW Advance Tech. Lab.
I Space Park
Redondo Beach, CA 90278

Prof. F. Chen
Department of Electrical Engineering
University of California at Los Angeles
Los Angeles, CA 90024

Dr. D. Chernin
Science Applications Intl. Corp.
1710 Goodridge Drive
McLean, VA 22102

Prof. R. Davidson
Plasma Fusion Center
M.I.T.
Cambridge, MA 02139

Dr. J. Dawson
University of California at Los Angeles
Department of Physics
Los Angeles, CA 90024

Dr. W.N. Destler
Department of Electrical Engineering
University of Maryland
College Park, MD 20742

Prof. W. Doggett
Physics Department
North Carolina State University
P.O. Box 8202
Raleigh, NC 27695

Dr. H. Dreicer
Director Plasma Physics Division
Los Alamos Scientific Laboratory
Los Alamos, NM 87544

Prof. W.E. Drummond
Austin Research Associates
1901 Rutland Drive
Austin, TX 78758

Dr. Don Eccleshall
Bldg. 120-Room 241
Ballistic Research Lab.
Aberdeen Proving Grounds
Aberdeen, MD 21005

Dr. J.G. Eden
Department of Electrical Engineering
University of Illinois
155 EEB
Urbana, IL 61801

Dr. A. Faltens
Lawrence Berkeley Laboratory
Berkeley, CA 94720

Dr. T. Fessenden
Lawrence Livermore National Laboratory
P.O. Box 808
Livermore, CA 94550

Dr. A. Fisher
Physics Department
University of California
Irvine, CA 92664

Prof. H.H. Fleischmann
Laboratory for Plasma Studies and
   School of Applied and Eng. Physics
Cornell University
Ithaca, NY 14850

Dr. T. Fowler
Associate Director
Magnetic Fusion Energy
Lawrence Livermore National Laboratory
P.O. Box 808
Livermore, CA 94550

Mr. George B. Frazier, Manager
Pulsed Power Research & Engineering Dept.
2700 Merced St.
P.O. Box 1538
San Leandro, CA 94577

LCDR W. Fritchie
Space and Naval Warfare
   Systems Command
Attention: Code PMW145B
Washington, DC 20363-5100

Dr. S. Graybill
Harry Diamond Laboratory
2800 Powder Mill Road
Adelphi, MD 20783

Lt. Col. R. Gullickson
SDIO-DEO
Pentagon
Washington, DC 20301-7100

Dr. Z.G.T. Guiragossian
TRW Systems and Energy RI/1070
Advanced Technology Lab
1 Space Park
Redondo Beach, CA 90278

Prof. D. Hammer
Laboratory of Plasma Physics
Cornell University
Ithaca, NY 14850

Dr. David Hasti
Sandia National Laboratory
Albuquerque, NM 87115

Dr. C.E. Hollandsworth
Ballistic Research Laboratory
DRDAB - BLB
Aberdeen Proving Ground, MD 21005

Dr. C.M. Huddleston
ORI
1375 Piccard Drive
Rockville, MD 20850

Dr. S. Humphries
University of New Mexico
Albuquerque, NM 87131

Dr. Robert Hunter
9555 Distribution Ave.
Western Research Inc.
San Diego, CA 92121

Dr. J. Hyman
Hughes Research Laboratory
3011 Malibu Canyon Road
Malibu, CA 90265

Prof. H. Ishizuka
Department of Physics
University of California at Irvine
Irvine, CA 92664

Dr. Donald Kerst
University of Wisconsin
Madison, WI 53706

Dr. Edward Knapp
Los Alamos Scientific Laboratory
Los Alamos, NM 87544

Dr. A. Kolb
Maxwell Laboratories
8835 Balboa Ave.
San Diego, CA 92123

Dr. Peter Korn
Maxwell Laboratories
8835 Balboa Ave.
San Diego, CA 92123

Dr. R. Linford
Los Alamos Scientific Laboratory
P.O. Box 1663
Los Alamos, NM 87545

Dr. C.S. Liu
Department of Physics
University of Maryland
College Park, MD 20742

Prof. R.V. Lovelace
School of Applied and Eng. Physics
Cornell University
Ithaca, NY 14853

Dr. S.C. Luckhardt
Plasma Fusion Center
M.I.T.
Cambridge, MA 02139

Dr. J.E. Maenchen
Division 1241
Sandia National Lab.
Albuquerque, NM 87511

Prof. T. Marshall
School of Engineering and Applied Science
Plasma Laboratory
S.W. Mudd Bldg.
Columbia University
New York, NY 10027

Dr. M. Mazarakis
Sandia National Laboratory
Albuquerque, NM 87115

Dr. D.A. McArthur
Sandia National Laboratories
Albuquerque, NM 87115

Prof. J.E. McCune
Dept. of Aero. and Astronomy
M.I.T.
77 Massachusetts Ave.
Cambridge, MA 02139

Prof. G.H. Miley, Chairman
Nuclear Engineering Program
214 Nuclear Engineering Lab.
Urbana, IL 61801

Dr. Bruce Miller
TITAN Systems
9191 Town Centre Dr.
Suite 500
San Diego, CA 92122

Dr. A. Mondelli
Science Applications, Inc.
1710 Goodridge Drive
McLean, VA 22102

Dr. Phillip Morton
Stanford Linear Accelerator Center
Stanford, CA 94305

Dr. M. Nahemow
Westinghouse Electric Corporation
1310 Beutah Rd.
Pittsburg, PA 15235

Prof. J. Nation
Lab. of Plasma Studies
Cornell University
Ithaca, NY 14850

Dr. V.K. Neil
Lawrence Livermore National Laboratory
P.O. Box 808
Livermore, CA 94550

Dr. Gene Nolting
Naval Surface Weapons Center
White Oak Laboratory
10901 New Hampshire Ave.
Silver Spring, MD 20903-5000

Dr. C.L. Olson
Sandia Laboratory
Albuquerque, NM 87115

Dr. Arthur Paul
Lawrence Livermore National Laboratory
P.O. Box 808
Livermore, CA 94550

Dr. S. Penner
Institute of Technology and Standards
Washington, D.C. 20234

Dr. Jack M. Peterson
Lawrence Berkeley Laboratory
Berkeley, CA 94720

Dr. R. Post
Lawrence Livermore National Lab.
P.O. Box 808
Livermore, CA 94550

Dr. Kenneth Prestwich
Sandia National Laboratory
Albuquerque, NM 87115

Dr. S. Prono
Los Alamos Scientific Lab.
Los Alamos, NM 87544

Dr. Sid Putnam
Pulse Science, Inc.
600 McCormick Street
San Leandro, CA 94577

Dr. Louis L. Reginato
Lawrence Livermore National Lab
P.O. Box 808
Livermore, CA 94550

Prof. N. Reiser
Dept. of Physics and Astronomy
University of Maryland
College Park, MD 20742

Dr. M.E. Rensink
Lawrence Livermore National Lab
P.O. Box 808
Livermore, CA 94550

Dr. D. Rej
Los Alamos Scientific Lab.
Los Alamos, NM 87544

Dr. J.A. Rome
Oak Ridge National Lab
Oak Ridge, TN 37850

Prof. Norman Rostoker
Dept. of Physics
University of California
Irvine, CA 92664

Prof. George Schmidt
Physics Department
Stevens Institute of Tech.
Hoboken, NJ 07030

Philip E. Serafim
Northeastern University
Boston, MA 02115

Dr. Andrew Sessler
Lawrence Berkeley National Lab
Berkeley, CA 94720

Dr. John Siambis
Lockheed
Palo Alto Research Lab
3257 Hanover Street
Palo Alto, CA 94304

Dr. Adrian C. Smith
Ballena Systems Corp.
1150 Ballena Blvd., Suite 210
Alameda, CA 94501

Dr. Lloyd Smith
Lawrence Berkeley National Laboratory
Berkeley, CA 94720

Dr. A. Sternlieb
Lawrence Berkely National Laboratory
Berkeley, CA 94720

Dr. D. Straw
W.J. Schafer Assoc.
2000 Randolph Road, S.E., Suite A
Albuquerque, NM 87106

Prof. C. Striffler
Dept. of Electrical Engineering
University of Maryland
College Park, MD 20742

Prof. R. Sudan
Laboratory of Plasma Studies
Cornell University
Ithaca, NY 14850

Dr. W. Tucker
Sandia National Laboratory
Albuquerque, NM 87115

Dr. H. Uhm
Naval Surface Weapons Center
White Oak Laboratory
10901 New Hampshire Ave. Code R41
Silver Spring, MD 20903-5000

Dr. William Weldon
University of Texas
Austin, TX 78758

Dr. Mark Wilson
Institute of Technology and Standards
Washington, DC 20234

Dr. P. Wilson
Stanford Linear Accelerator Center
Stanford, CA 94305

Prof. C.B. Wharton
303 N. Sunset Drive
Ithaca, NY 14850

Dr. Gerald Yonas
Sandia National Lab.
Albuquerque, NM 87115

Naval Research Laboratory
Washington, DC 20375-5000
Code 1220

Naval Research Laboratory
Washington, DC 20375-5000
Code 4830
Timothy Calderwood

Director of Research
U.S. Naval Academy
Annapolis, MD 21402
(2 copies)

West Defense Technical Information Center - 2 copies

NRL Code 1000 - 1 copy

NRL Code 10001 - 1 copy

NRL Code 2628 - 20 copies

NRL Code 4000 - 1 copy

NRL Code 4001 - 1 copy

NRL Code 4700 - 26 copies

NRL Code 4701 - 1 copy

NRL Code 4790 - 1 copy

NRL Code 4795 - 40 copies

Do NOT make labels for
    Records----(01 cy)
    Code 4828--(22 cys)

MAILING LIST/FOREIGN

Library
Institut fur Plasmaforschung
Universitat Stuttgart
Pfaffenwaldring 31
7000 Stuttgart 80, West Germany

Ken Takayama
KEN, TRISTAN Division
Oho, Tsukuba, Ibaraki, 305 JAPAN